Chapter 2

DNA-modified Electrodes Fabricated using Copper-Free Click Chemistry for Enhanced Protein Detection

Adapted from: Furst, A. L., Hill, M. G., and Barton, J. K. (2013) DNA-Modified Electrodes Fabricated Using Copper-Free Click Chemistry for Enhanced Protein Detection, *Langmuir*, *29*, 16141-16149.

Introduction

Sensitive detection of biomarkers is essential for the development of effective diagnostic tools. Electrochemical biosensing platforms have the unique ability to convert biological events, including protein or ligand binding and DNA or RNA hybridization, directly into electronic signals, making them ideal tools for point-of-care diagnostics.[1-7] The ability of DNA to conduct charge, and more specifically, the sensitivity of DNA charge transport (DNA CT) to structural perturbations of the double helix, provides a robust signaling mechanism for DNA-modified electrode-based biosensing.[8] Exploiting DNA CT, we have developed highly sensitive electrochemical assays for nucleic acids and protein-DNA binding.[9-14]

Typically, DNA-modified surfaces are prepared through self-assembly of thiolated DNA duplexes on gold to form high-density monolayers. While straightforward to fabricate, these films pose challenges for the detection of very large proteins, proteins that target specific sequences of DNA, and hybridization/dehybridization events, owing to the limited accessibility to individual helices within the close-packed structure of the monolayer.[15, 16] Although some control over the surface density is possible by adjusting the ionic strength of the deposition solution with magnesium ions, the range of attainable DNA surface coverages is narrow (~ 30 – 50 pmol/cm^2).[17-20] Moreover, this method does not allow for control over the dispersion of DNA helices within the film; recent imaging studies have revealed that thiol-modified DNA forms a heterogeneous monolayer when combined with a passivating agent such as mercaptohexanol. In such films, the DNA helices cluster into exceedingly large domains of very high density within a sea of passivating thiol.[21, 22] This extensive clustering of helices is especially problematic for

biomolecule detection because it leads to variability across the electrode surface, with regions of close-packed helices in which access to specific base sequences may be inhibited.

The structural similarity of the components of a mixed monolayer-forming solution is a major determining factor for the degree of homogeneity within the resulting self-assembled monolayer (SAM).[23-29] Thus an alternative approach to a low-density DNA film is to prepare a homogeneous mixed SAM *without* DNA, followed by DNA conjugation to the functionalized mixed monolayer. Previous work by Chidsey and coworkers involved the preliminary formation of a mixed alkylthiol monolayer on gold containing azide-terminated thiols, followed by copper-catalyzed click chemistry to tether single-stranded oligonucleotides to gold surfaces. While copper-catalyzed click chemistry is efficient,[30] conventional copper(I) catalysts can damage DNA and are difficult to remove after the reaction has occurred.

In this work, we employ a catalyst-free method of DNA conjugation to a mixed monolayer that capitalizes on ring strain to drive the [3+2] cycloaddition.[31, 32] We first form a mixed azide-alcohol-terminated monolayer, then add cyclooctyne-labeled DNA, which, due to ring strain, spontaneously couples specifically to the azide. Because the loading and distribution of DNA are pre-fixed by the composition of the underlying monolayer, this labeling method enables very low surface concentrations of DNA to be evenly dispersed across the electrode, as verified by AFM imaging, and provides a significantly larger surface area-to-volume ratio for the DNA, increasing the accessibility of analyte in solution to individual helices. These low-density monolayers display all of the characteristics of DNA-mediated electrochemistry, including sensitivity to

mismatches and π-stack perturbations. Furthermore, the enhanced sensitivity of these monolayers to protein binding (as compared to conventional DNA-modified electrodes) makes them attractive platforms for biomolecule detection.

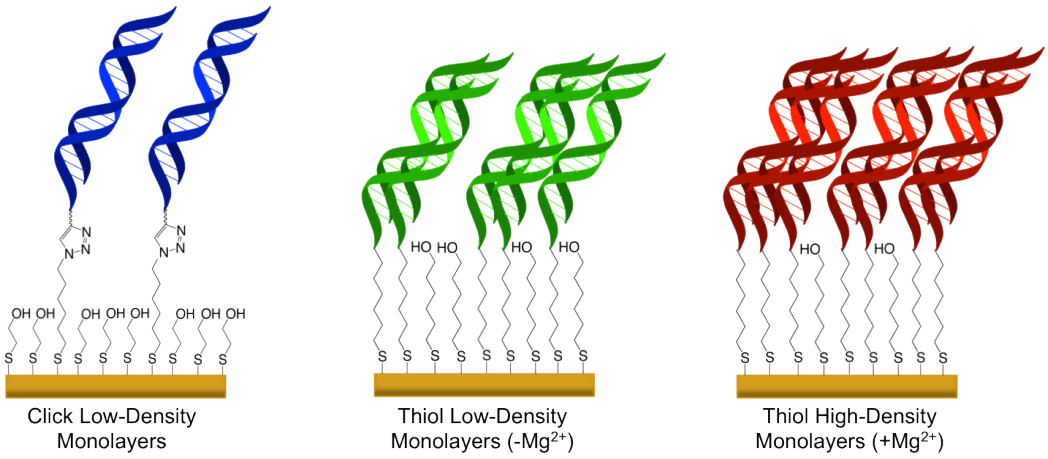

Figure 2.1 DNA monolayers of different densities. The ultra low-density DNA monolayers (*left*) are formed using click chemistry on surfaces. Both low-density DNA monolayers (*center*) and high-density DNA monolayers (*right*) are formed with self-assembly of thiolated DNA on surfaces. Click chemistry leads to significantly more homogeneous monolayers than either the low- or high-density thiol DNA monolayers.

Materials and Methods

Synthesis of NHS Ester Activated Cyclooctyne

9,9-Dibromobicyclo-[6.1.0]nonane was synthesized according to the procedure by Skattebøl et al.[33] The cyclooctyne was synthesized as described by Agard et al.[27] Cyclooctyne (OCT) was prepared for coupling to DNA by NHS ester activation. 5 mg (0.019 mmol) of OCT was combined with 7 mg (0.034 mmol) N,N'-dicyclohexylcarbodiimide and 3.7 mg (0.033 mmol) N-hydroxysuccinimide in 1 mL anhydrous DMF. The reaction was stirred for 1.5 h, followed by solvent removal under reduced pressure.

Oligonucleotide Synthesis and Purification

Oligonucleotides were synthesized on an Applied Biosystems 3400 DNA synthesizer. Terminal modifications incorporated into the 5' end of one of the strands were either a C6 S-S thiol linker or a C3 amine linker, purchased from Glen Research. Complementary unmodified strands were also synthesized. Each oligonucleotide was purified by high-performance liquid chromatography (HPLC) using a gradient of acetonitrile and 50 mM ammonium acetate. Preparation of all of the oligonucleotides followed a reported protocol.[34] Following purification, oligonucleotides were desalted by ethanol precipitation and quantified using ultraviolet-visible spectrophotometry based on their extinction coefficients at 260 nm (IDT Oligo Analyzer). The following sequences were prepared: well matched: 5'-NH_3-$(CH_2)_3$-GCT CAG TAC GAC GTC GA-3' with its unmodified complement, a mismatch-containing sequence with a CA mismatch at the 9th base pair, and a TBP-binding sequence: 5'-NH_3-$(CH_2)_3$-GGC GTC TAT AAA GCG

ATC GCG A-3' with its unmodified complement. DNA to be coupled to OCT was synthesized with a 5'-terminal C3 amino-modifier. The DNA was cleaved from solid support, deprotected, and HPLC-purified as previously described. The OCT-NHS ester was suspended in 20 uL of dry DMSO in preparation for coupling to DNA. Following desalting, the oligonucleotides were suspended in 100 μL of 0.5 M $NaHCO_3/Na_2CO_3$ buffer (pH 8.75) and the OCT-ester in DMSO was added to the oligonucleotides. The reaction was stirred for 24 h, followed by a final round of HPLC purification. The formation of the desired product was confirmed by a significant shift in the HPLC retention time and MALDI-TOF analysis of the product. MALDI-TOF: calc: 5592.1 obs: 5589.08.

DNA duplexes were formed by thermally annealing equimolar amounts of single-stranded oligonucleotides in deoxygenated phosphate buffer (5mM phosphate, 50 mM NaCl, pH 7.0) at 90° C for 5 minutes followed by slowly cooling to 25° C.

AFM Measurements

Silicon AFM tips (Nanosensors™ AdvancedTEC™) with a force constant of 0.2 N were first chemically modified by vapor deposition of a 10-nm layer of gold using a CVC Metal Physical Evaporator Deposition system, followed by soaking in a 10 mM solution of hexanethiol in ethanol for 1 h. Modified tips were thoroughly rinsed with 200-proof ethyl alcohol before use.

Scanning probe microscopy (SPM) images were acquired with a MultiMode Scanning Probe Microscope (Digital Instruments). DNA-modified surfaces were mounted on the SPM, and all images were collected with contact mode in phosphate

buffer (50 mM, pH 7.0) at ambient temperature. To obtain height measurements of the monolayers, a voltage of 10 V was applied to the tip, which was scanned repetitively over a 1 μm square area to physically remove the adsorbed monolayer. A portion of the mixed monolayer was removed, followed by measuring the depth profile of the hole produced. Holes were formed on several independent surfaces, and the height profiles of ten different holes were measured (Figure 2.2).

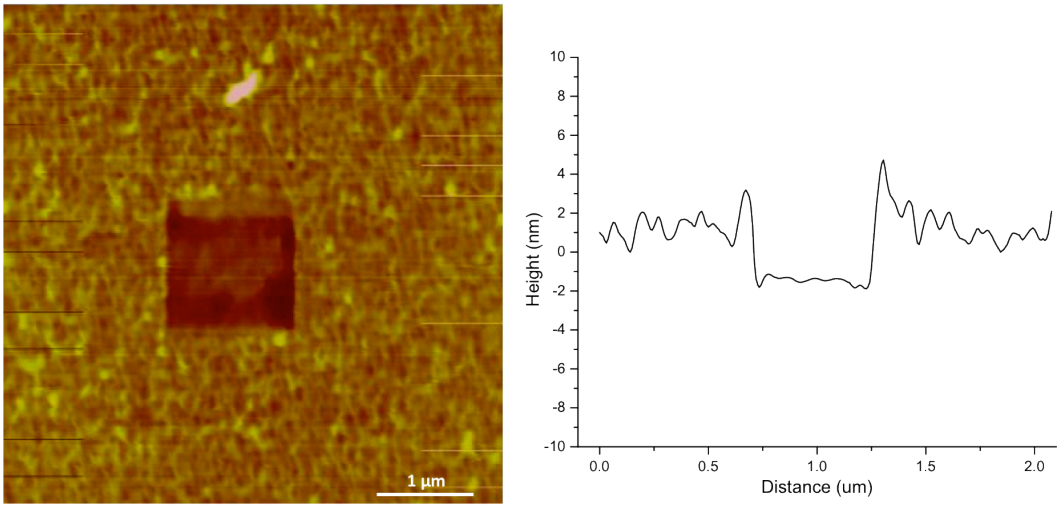

Figure 2.2 Depth measurement of OCT-DNA monolayer with AFM. The image shown is obtained in phosphate buffer (5 mM phosphate, 50 mM NaCl, pH 7.0) with a chemically-modified AFM tip. A hole is formed through the application of a force to the AFM tip in contact mode. When a force is no longer applied to the tip, the depth of the resulting hole is measured. When averaged over many measurements, the height of the monolayer is determined to be 3.5 nm.

Preparation of DNA-Modified Electrodes and AFM Surfaces

Stationary gold electrodes (1.6-mm diameter, BASi) and rotating disk electrodes, RDEs (5-mm diameter, Pine Instruments), were prepared for DNA monolayer formation by polishing with 0.05 μm alumina, followed by electrochemical cycling in 0.5 M H_2SO_4 between ~1.7 and -0.4 V.

High-density thiol-terminated DNA monolayers were formed by depositing 10 μL of 25 μM duplexed DNA in 5 mM phosphate buffer (pH 7.0) containing 100 mM $MgCl_2$ onto the electrode. The films were allowed to assemble for 12 h; the electrodes were then washed with phosphate buffer (5 mM phosphate, 50 mM NaCl, pH 7.0). The electrodes were subsequently backfilled with 1 mM 1-mercaptohexanol (MCH) in a 95:5 phosphate buffer (5 mM phosphate, 50 mM NaCl, pH 7.0)/glycerol solution for 45 minutes. The electrodes were again rinsed with phosphate buffer to ensure removal of residual MCH.

Monolayers featuring DNA-OCT were prepared using a two-step process. An initial mixed monolayer of mercaptoethanol (MCE) as the passivating agent and 6-Azido-1-hexanethiol ("thiol-azide") was formed by soaking the electrodes in an ethanol solution containing 1 mM MCE and 0.25 mM azide for 24 hours to form a monolayer composed of 20% azide. After washing with 5 mM phosphate buffer (pH 7.0), 10 μL of 50 μM DNA-OCT hybridized to its complement was deposited onto the electrode or gold AFM surface (Novascan), where the conjugation reaction was allowed to proceed for 24 hours before washing with phosphate buffer. The average DNA domain size of 25 nm was determined by measuring 15 islands on three different images, each 1 square micron in size.

Electrochemical Measurements

Electrochemical measurements were performed with a CH760B Electrochemical Analyzer (CH Instruments) using a AgCl/Ag reference electrode and Pt-wire counter electrode. Electrochemical measurements were recorded in the dark at ambient temperature in deoxygenated Tris buffer (10 mM Tris, 100 mM KCl, 2.5 mM $MgCl_2$, 1 mM $CaCl_2$, pH 7.6). Using methylene blue, covalently attached to the DNA by either a 2-carbon or 6-carbon alkyl tether, no electrochemical signal decrease was observed upon incorporation of a single base mismatch, indicating that signals are dominated by interactions of the probe with the passivating layer. Additionally, signals obtained from a covalent Nile blue reporter were too small to quantify. Daunomycin (MPBio) dissolved to a final concentration of 2 μM in Tris buffer (10 mM Tris, 100 mM KCl, 2.5 mM $MgCl_2$, 1 mM $CaCl_2$, pH 7.6) was successfully used as a redox probe. All of the DNA sequences used for electrochemical measurements contain a terminal GC sequence, the preferred intercalation site for daunomycin, to direct the redox probe to the terminus of the helix, thereby maximizing the electrochemical effects of helical distortions including incorporation of mismatches and protein binding events. At daunomycin concentrations higher than 6 μM, the DNA-free films exhibited weak surface signals. All experiments were therefore carried out with concentrations of daunomycin at 2 μM, above the saturation limit for DNA intercalation but well below the binding concentration to the mixed-monolayer surface.

TBP Binding Measurements

TATA-Binding Protein (TBP) was purchased from ProteinOne and stored at -80° C until use. MicroBiospin 6 columns (BioRad) were used to exchange the shipping buffer for Tris buffer (10 mM Tris, 100 mM KCl, 2.5 mM $MgCl_2$, 1 mM $CaCl_2$, pH 7.6). Prior to electrochemical measurements with TBP, electrodes were incubated with 1 μM Bovine serum albumin (BSA) for 30 min, followed by rinsing with Tris buffer. BSA binds non-specifically to modified electrodes, which acts to coat any regions where such non-specific binding could occur before the addition of TBP. Electrodes were scanned in the dark in deoxygenated Tris buffer (10 mM Tris, 100 mM KCl, 2.5 mM $MgCl_2$, 1 mM $CaCl_2$, pH 7.6) with 2 μM daunomycin and, unless otherwise noted, 150 nM TBP. In the case of RDEs, unless otherwise noted, electrodes were rotated at 400 rpm.

Results and Discussion

Formation of Low-Density Monolayers by Copper-Free Click Chemistry

Conventional DNA-modified electrodes are prepared by self-assembling thiol-modified DNA duplexes onto gold, followed by backfilling with an alkylthiol to passivate any remaining exposed surface. This method leaves little room for control over the density and spacing of the DNA molecules.[21, 22] Instead, we have labeled DNA with a cyclooctyne moiety (OCT) tethered to the 5' phosphate backbone (Figure 2.3); gold electrodes are then modified with an alcohol-terminated monolayer doped with an azide-capped alkyl thiol, followed by a copper-free click reaction in which cyclooctyne-labeled duplexes, OCT-DNA, are coupled to the film *via* azide-alkyne cycloaddition.[35] This approach offers several advantages over conventional preparations of DNA monolayers: (i) it allows for precise control over the total amount of DNA by simply changing the fraction of thiol-azide present in the preliminary monolayer; (ii) the preliminary self-assembly step results in a passivated surface before the addition of DNA, minimizing undesirable direct interactions between the gold surface and DNA helices; and (iii) because the underlying azide conjugation sites are more evenly distributed in the preliminary monolayer, DNA helices are less prone to cluster into large, high-density domains.

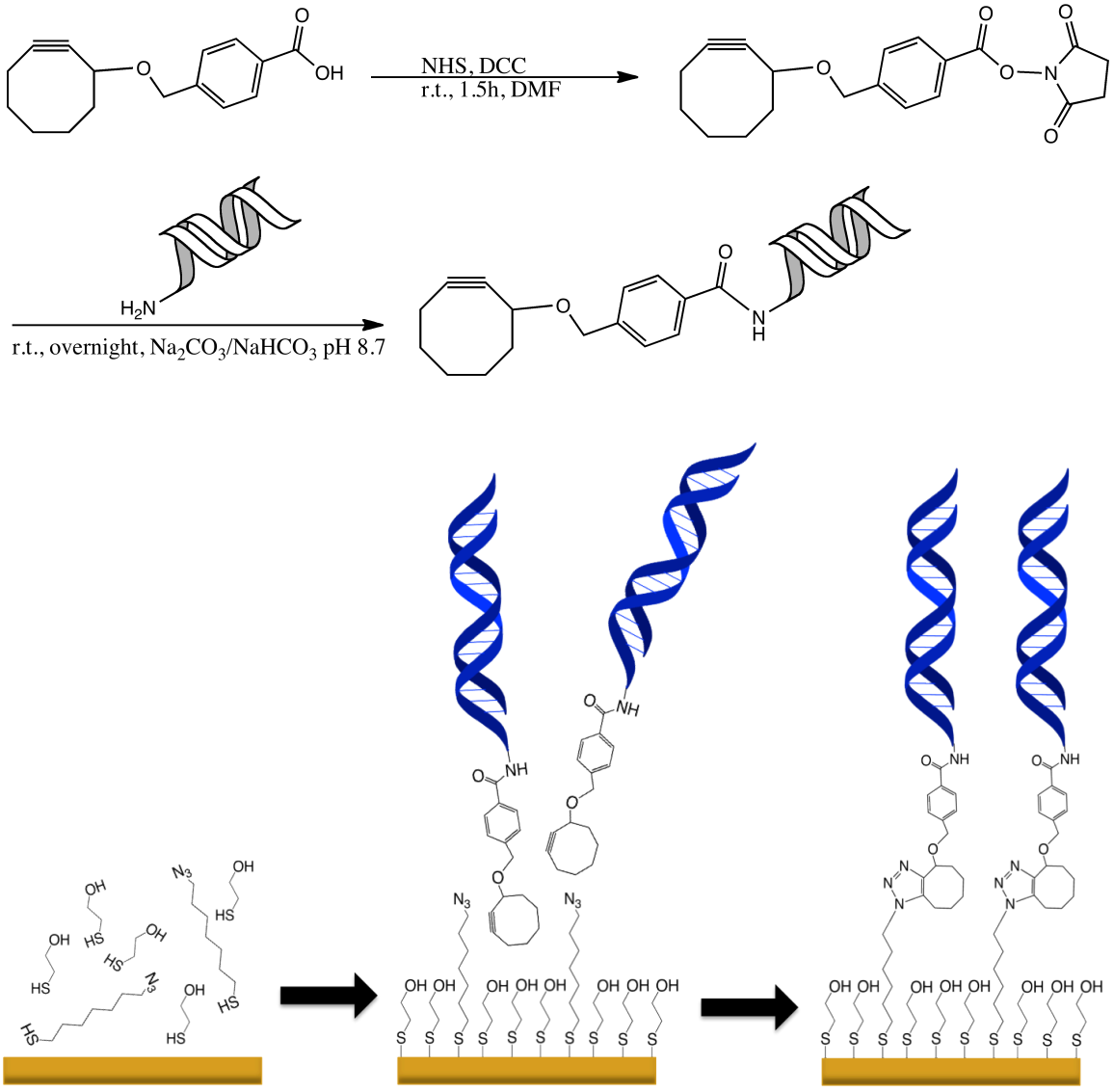

Figure 2.3 Synthesis of OCT-DNA and assembly of OCT-DNA monolayers. *(Above)* Synthetic scheme for OCT-DNA. *(Below)* A preliminary mixed monolayer of alcohol- and azide-terminated thiols is assembled on a gold surface. OCT-modified DNA is subsequently added and allowed to react with the azides to form a covalently tethered low-density DNA monolayer on gold.

Monolayer Characterization through AFM Imaging

OCT-DNA monolayers were examined by atomic force microscopy (AFM) under fluid conditions to visualize the DNA surface coverage and distribution of individual helices within the film. Previous AFM work on high-density monolayers revealed that DNA adheres to standard AFM tips, leading to disturbance of the DNA monolayer when the instrument is in contact mode.[18, 21, 22] We therefore employed tips modified with a hydrophobic film (mercaptohexane), which diminishes interactions with both the buffer and the negatively charged DNA on the surface.[18]

In contrast to low-density thiolated DNA monolayers, which show images consistent with quite densely packed monolayers,[21] images of OCT-DNA films on a 20% azide monolayer reveal no large-domain clustering (Figure 2.4). Notably, the images do show some monolayer stratification, consistent with extremely small clusters of DNA that are remarkably uniform in size and shape. Indeed, these mini-clusters likely indicate some sequestration of azide-thiol reagents in the underlying monolayer, presumably a result of small chain-length differences between the passivating molecules and the azide-containing thiols. While longer alcohol-terminated thiols were tested in an attempt to form a more evenly-dispersed mixed monolayer, DNA coupling efficiencies were extremely low for 3, 4, 5, and 6-carbon alcohol-terminated thiols, likely due to the size of the cyclooctyne.

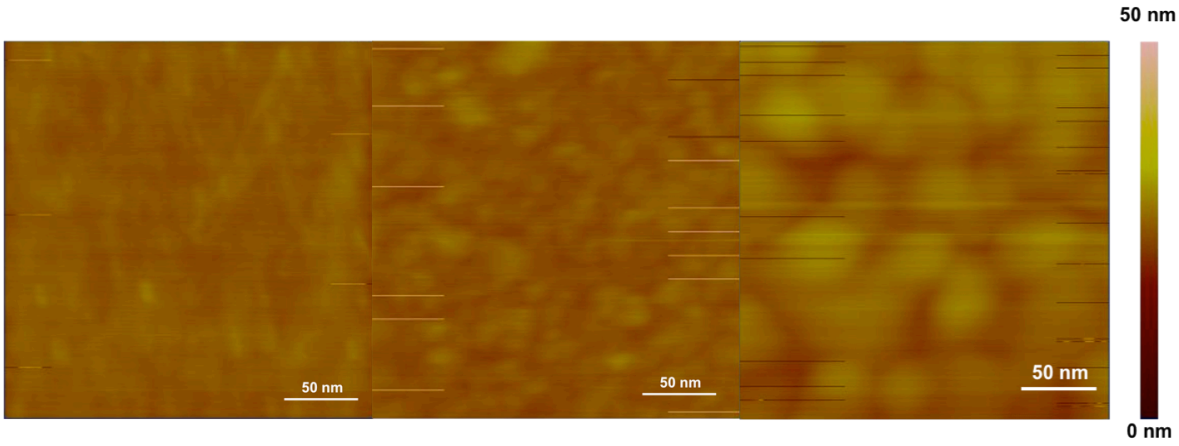

Figure 2.4 AFM images of the assembly of low-density OCT-DNA monolayers. Images are in phosphate buffer (5 mM phosphate, 50 mM NaCl, pH 7.0) and were obtained with chemically modified tips. *(Left)* Image of bare gold electrode. *(Center)* Self-assembled monolayer containing 20% thiol azide and 80% mercaptoethanol. *(Right)* Surface after incubation with OCT-DNA. The morphology of the surface changes with sequential modification steps. From the image on the right, it can be seen that the individual clusters of DNA on the surface are small; the number of DNA helices contained in a microcluster is approximately 150.

The height of these low-density DNA monolayers was also measured by AFM; we previously reported a film depth for densely packed 15-base-pair duplexes on gold of ~4.5 nm.[18] Analogous films prepared from OCT-DNA yield an average film height of ~3.5 nm ± 0.5 nm, consistent with a monolayer composed of a mixture of taller DNA mini-clusters and shorter underlying passivating agent (Figure 2.2). Notably, these regularly spaced bumps observed in the film-height profile are consistent with small aggregates of DNA homogeneously dispersed within the passivating film. The area of these bumps, attributed to mini-clusters of DNA, can be quantified. Based on the diameter of B-form DNA (2.0 nm) and the average diameter of the clusters (25 nm, an average of the size of clusters measured from three 1 μm^2 AFM images), each cluster contains ~ 150 individual helices, with the overall DNA surface coverage for the entire AFM field of view estimated as ~15 pmol/cm^2. Significantly, this implies that ~1/3 of the duplexes in the film have a solution-exposed edge, meaning that a much greater portion of DNA in these monolayers is directly accessible to analytes in solution as compared to films in which the DNA helices are closely packed into large islands.

Electrochemical Monolayer Characterization

OCT-DNA monolayers (5% - 90% azide in the underlying film) were also examined using electrochemical assays. For 20% azide films, the total surface coverage of DNA, G_{DNA}, was measured based on the electrochemical response of $Ru(NH_3)_6^{3+}$ electrostatically bound to the DNA.[20, 36, 37] 20% azide films that featured fully Watson-Crick base-paired duplexes, as well as 20% azide films with duplexes that possessed a single CA mismatch, were investigated. Voltammetry of micromolar solutions of

$Ru(NH_3)_6^{3+}$ yielded well defined $Ru^{3+/2+}$ surface waves; integrating the traces yielded an average value for DNA surface coverage of 13.5±1 pmol/cm^2, as determined by Eq.1 (where *z* is the charge on ruthenium, 3+, and *m* is the number of nucleotides in the duplex, 17).

$$\Gamma_{DNA} = \Gamma_{Ru}\left(\frac{m}{z}\right) \qquad (1)$$

This surface coverage is not only in excellent agreement with that calculated by AFM, but is the same regardless of whether the monolayers are formed from well matched or mismatched OCT-DNA duplexes. In comparison, high-density monolayers prepared from thiol-labeled DNA typically yield surface coverages in the range of 40 - 50 pmol/cm^2.[38] These data show that the coupling on a surface is essentially quantitative, as a preliminary monolayer composed of 20% azide yields a total DNA coverage that is 25% of the coverage of high-density monolayers, as measured with $Ru(NH_3)_6^{3+}$. Significantly, the amount of DNA on the surface increased linearly with the percentage of azide used to form the underlying monolayer (Figure 2.5). As the amount of DNA increased linearly with increasing solution concentrations of azide, the solution percentage of azide appears proportional to the amount that assembles on the electrode, which also indicates that OCT-DNA coupling appears essentially quantitative.

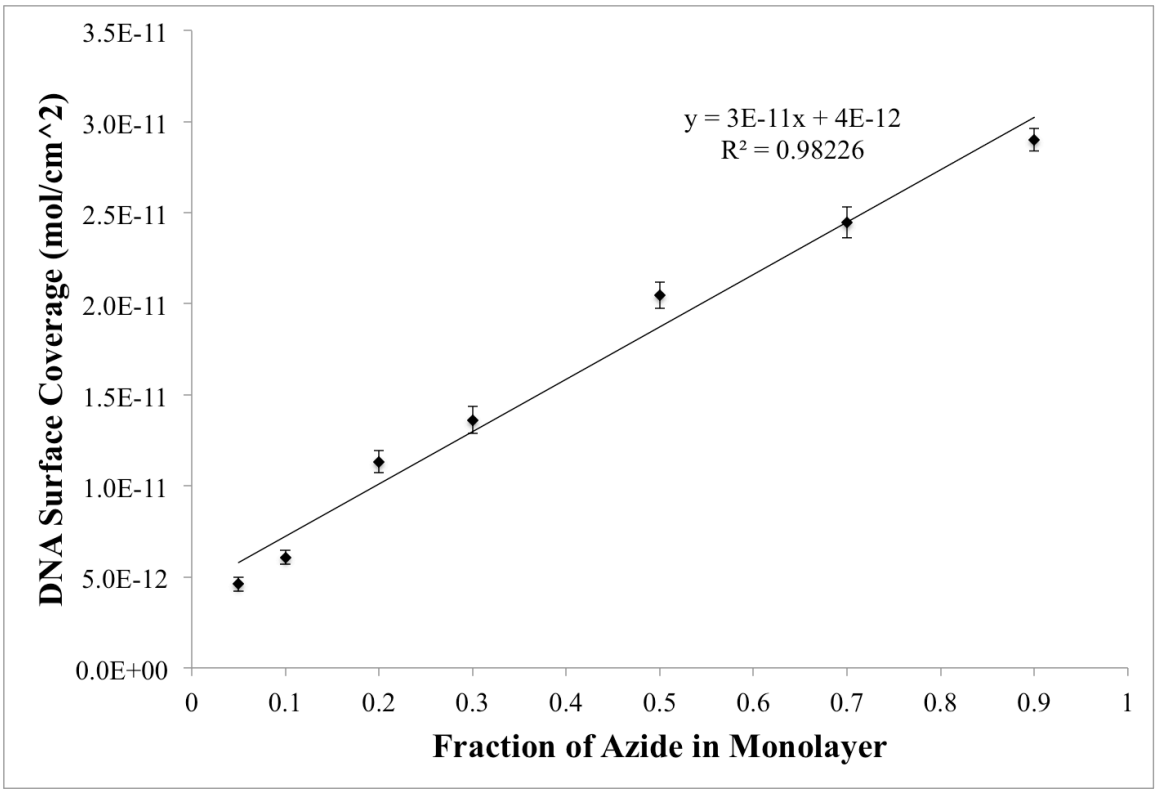

Figure 2.5 Quantification of DNA in OCT-DNA monolayers assembled with varying solution concentrations of azide. The amount of OCT-DNA that covalently attached to monolayers formed with varying concentrations of azide in the monolayer formation solution was determined by measuring electrochemical signals in a 20 μM ruthenium hexammine solution in Tris buffer (10 mM Tris, 100 mM KCl, 2.5 mM $MgCl_2$, 1 mM $CaCl_2$, pH 7.6). Concentrations of azide ranged from 5%-90%. A linear increase in amount of DNA on the surface with increasing percent of azide indicates that the solution concentration of azide is a valid approximation of the amount of azide assembled in the monolayer, and that the DNA coupling to the active head groups on the surface is essentially quantitative.

To assess OCT-DNA films for DNA CT-based biosensing applications, we carried out experiments using non-covalent intercalative probe molecules.[13] The anthraquinone-based drug daunomycin (DM) intercalates into DNA films where it undergoes a reversible 1 e^- reduction at pH values greater than ~7.3.[11, 39, 40] Figure 2.6 shows the background-subtracted cyclic voltammogram of DM at a well-matched OCT-DNA surface. Significantly, no signal is observed under identical conditions at a mixed alcohol/azide monolayer, confirming that the observed DM signals are due to the presence of intact DNA. Moreover, the presence of an intervening CA mismatch results in nearly complete loss of the DM electrochemical response, yet the electrode maintains a nearly identical $Ru(NH_3)_6^{3+}$ redox signal. This confirms that the attenuation of the DM signals at mismatched OCT-DNA is not due to dehybridization or less favorable monolayer assembly.

While DM undergoes efficient oxidation and reduction when intercalated into well-matched OCT-DNA duplexes, the incorporation of an intervening CA mismatch results in nearly complete loss of the electrochemical response (see Figures 2.6, 2.7). This sensitivity to mismatches is strong evidence for a DNA-mediated CT reaction. Importantly, both well matched and mismatched OCT-DNA films yield virtually identical $Ru(NH_3)_6^{3+}$ responses (Figure 2.6), confirming that the attenuation of the DM signals at mismatched OCT-DNA is not due to dehybridization or less favorable assembly of the mismatched monolayer versus the matched.

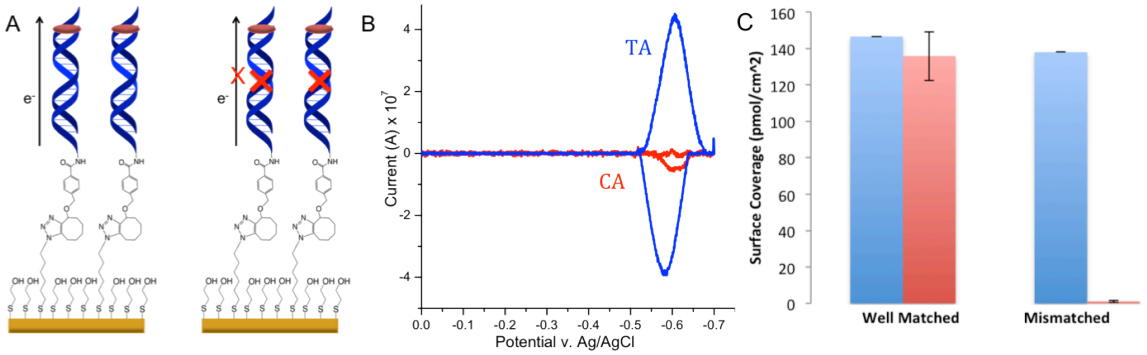

Figure 2.6 Electrochemical mismatch discrimination. (A) The incorporation of a single-base mismatch into the sequence of DNA assembled on an electrode prevents electrons from flowing to the redox probe as compared to the electron flow through the well-matched DNA. (B) A background-subtracted cyclic voltammogram (CV) of the electrochemical signal discrimination observed between well-paired helices in an OCT-DNA monolayer (blue) and an OCT-DNA monolayer with DNA containing a CA mismatch (red) is shown. The CV was obtained with a scan rate of 100 mV/s. Both DNA duplexes were 17 base pairs in length. Traces were obtained with 2 μM daunomycin in Tris buffer (10 mM Tris, 100 mM KCl, 2.5 mM $MgCl_2$, 1 mM $CaCl_2$, pH 7.6). Almost a complete signal loss is observed upon incorporation of a single CA mismatch. (C) DNA CT mismatch discrimination compared to quantified DNA surface coverage. The surface coverage determined from the DNA-mediated electrochemical signal obtained from daunomycin for well matched DNA and DNA containing a single-base mismatch (blue) is compared to coverage determined from the electrochemical signal of ruthenium hexammine (red), which electrostatically interacts the phosphates in the DNA and does not report on helix integrity. Surface coverages were calculated from the quantification of the area of the anodic peak of a CV obtained for both reporters at a scan rate of 100 mV/s in Tris buffer Tris buffer (10 mM Tris, 100 mM KCl, 2.5 mM $MgCl_2$, 1 mM $CaCl_2$, pH 7.6). Almost identical amounts of DNA are present for the well matched and mismatched sequences as quantified with ruthenium hexammine; the only observable difference is in the DNA-mediated daunomycin signal. Error bars are given for the standard deviation from three replicates for each experimental condition.

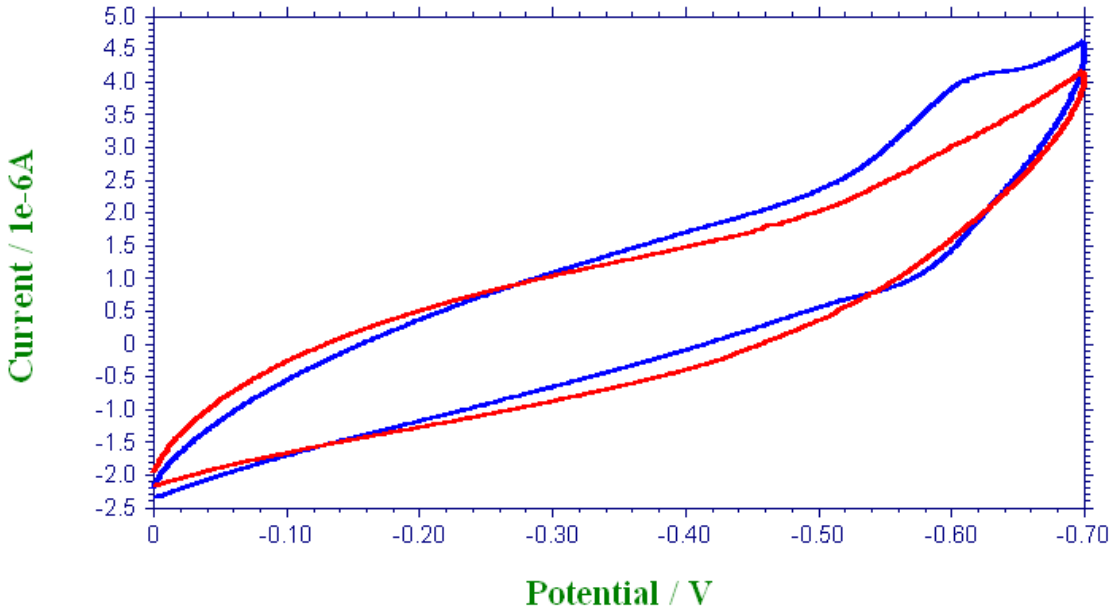

Figure 2.7 Raw cyclic voltammogram (CV) of mismatch discrimination. The electrochemical signal discrimination observed between well-paired helices in an OCT-DNA monolayer (blue) and an OCT-DNA monolayer with DNA containing a CA mismatch (red) is shown. The background-subtracted CV is shown in an additional figure. The CV was obtained with a scan rate of 100 mV/s. Both DNA duplexes were 17 base pairs in length. Traces were obtained with 2 μM daunomycin in Tris buffer (10 mM Tris, 100 mM KCl, 2.5 mM $MgCl_2$, 1 mM $CaCl_2$, pH 7.6). Almost a complete signal loss is observed upon incorporation of a single CA mismatch.

Electrochemistry of TBP Binding

To test whether the enhanced solution accessibility of DNA helices in OCT-DNA films allows for improved protein detection, we investigated the binding of TATA-binding protein, TBP. The electrochemistry of DM at OCT-DNA films with 20%, 50% and 90% azide, as well as conventional low- and high-density films in which the individual helices contained a TATA sequence, were examined in the presence of TBP. TBP, a subunit of the TFIID transcription factor in eukaryotes, kinks DNA (80°) when bound to its TATA target sequence and has been shown to attenuate DNA CT on DNA-modified electrodes.[11, 13, 41, 42] Before incubation with TBP, monolayers were incubated with BSA, a non-DNA binding protein. This protein adheres non-specifically to the electrode surfaces, ensuring that electrochemical changes after TBP addition are due to the specific binding of TBP to DNA.

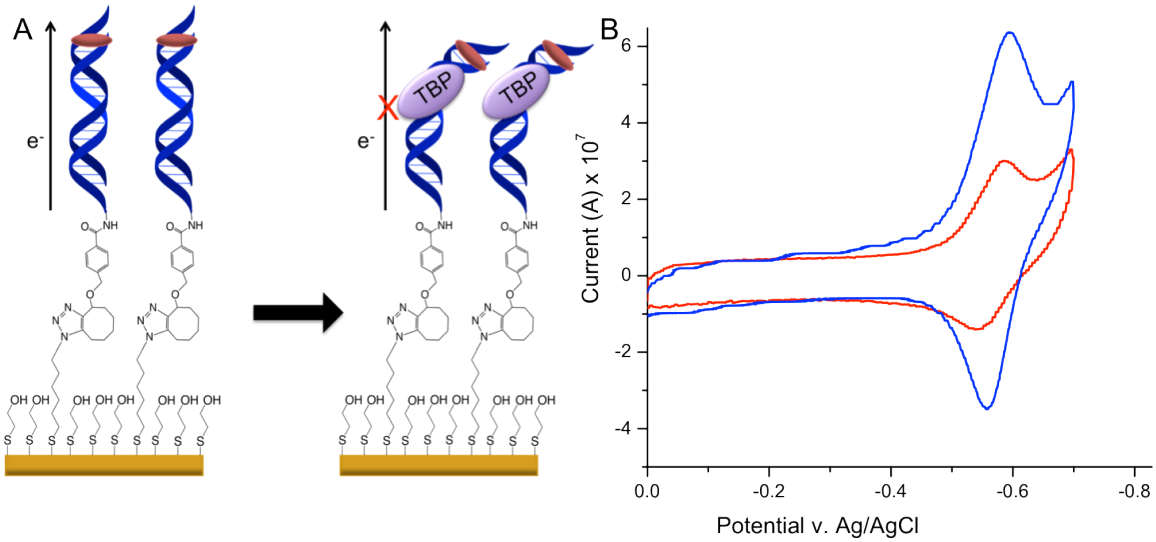

Figure 2.8 Electrochemical determination of TBP binding. *(A)* The binding and subsequent kinking of DNA by TBP prevents electrons from flowing to the daunomycin redox probe; before the protein is bound, there is a significant amount of electron flow through the DNA. *(B)* A cyclic voltammogram (CV) of the electrochemical signal reduction observed in an OCT-DNA monolayer with the TBP binding DNA sequence before the addition of protein (blue) and after the addition of 150 nM TBP that is allowed to incubate for 15 minutes (red) is shown. The CV was obtained with a scan rate of 100 mV/s. The TBP binding DNA duplex is 22 base pairs in length. Traces were obtained with 2 μM daunomycin in Tris buffer (10 mM Tris, 100 mM KCl, 2.5 mM $MgCl_2$, 1 mM $CaCl_2$, pH 7.6). Significant signal attenuation is observed upon TBP binding.

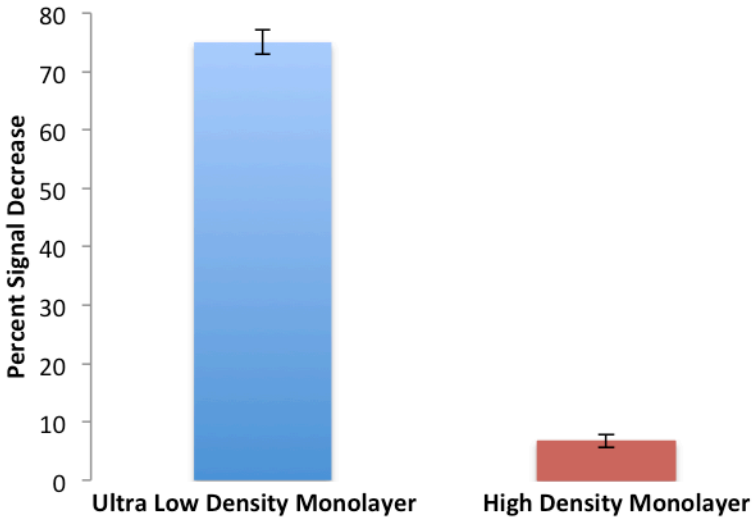

Figure 2.9 Percent signal decrease upon TBP binding for high- versus low-density DNA monolayers. Shown is the percent signal decrease from the DNA-mediated electrochemical signal obtained from daunomycin for TBP binding to DNA in an OCT-DNA monolayer (blue) and a high-density thiol monolayer (red) after addition of 75 nM TBP. Percent signal decreases are calculated from the quantification of the area of the anodic peak of a CV obtained for the signal before and after TBP addition at a scan rate of 100 mV/s in Tris buffer (10 mM Tris, 100 mM KCl, 2.5 mM $MgCl_2$, 1 mM $CaCl_2$, pH 7.6). Error bars are given for the standard deviation from three replicates.

No significant change in electrochemical signal was observed with either the well-matched sequence or the TBP-binding sequence after BSA incubation. After subsequent incubation with TBP, the presence of 150 nM protein causes a signal decrease of 75% at OCT-DNA films (20% azide), compared to a decrease of only 6% at high-density monolayers (Figures 2.8, 2.9). The preliminary addition of BSA ensures that ensuing signal decreases upon TBP addition are due to the specific binding of the protein. To further confirm that the signal decrease was due to a loss of DNA CT caused by TBP binding and subsequent kinking of the DNA, we measured the $Ru(NH_3)_6^{3+/2+}$ response, which gave nearly identical values for G_{DNA} regardless of whether the OCT-DNA sequences were matched, mismatched, or contained the TATA binding sequence (Figure 2.10).

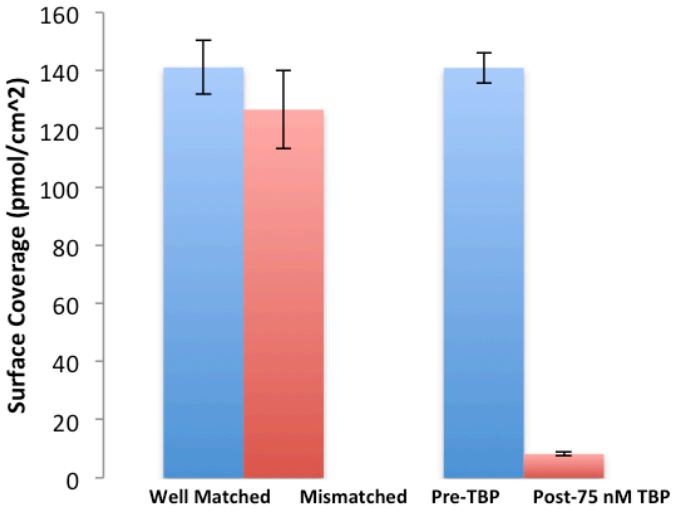

Figure 2.10 TBP DNA CT signal attenuation compared to quantified DNA surface coverage on an OCT-DNA monolayer. In red is the surface coverage determined from the DNA-mediated electrochemical signal obtained from daunomycin for the TBP binding DNA sequence before and after the addition of 75 nM TBP. In blue is the surface coverage determined from the electrochemical signal of ruthenium hexammine, which electrostatically interacts with the phosphates in the DNA and does not report on helix integrity. Surface coverages are calculated from the quantification of the area of the anodic peak of a CV obtained for both reporters at a scan rate of 100 mV/s in Tris buffer (10 mM Tris, 100 mM KCl, 2.5 mM $MgCl_2$, 1 mM $CaCl_2$, pH 7.6). As can be seen from the graph, the amount of DNA on the surface does not change upon addition of TBP, as quantified with ruthenium hexammine; the only observable difference in coverage is in the DNA-mediated daunomycin signal. Error bars are given for the standard deviation from three replicates for each experimental condition.

We also investigated detection limits of TBP binding at OCT-DNA films through the titration of TBP onto DNA-modified electrodes comprised of both OCT- and thiol-modified DNAs (Figure 2.11). Films formed from OCT-DNA are significantly more sensitive to TBP. A signal attenuation of over 10% is observed for both the 20% and 50% azide monolayers upon addition of 4 nM TBP protein, a concentration near the dissociation constant of TBP. The ability to detect proteins at such low concentrations is an important step in the development of DNA-modified films for diagnostic applications.

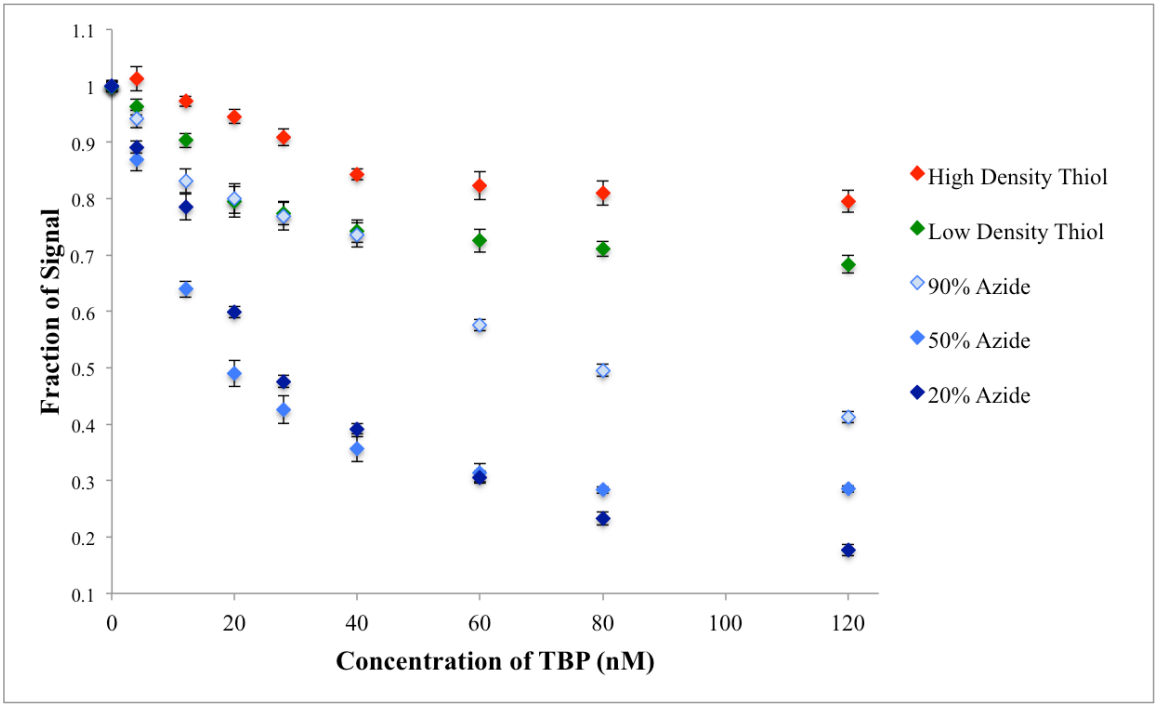

Figure 2.11 TBP titration onto DNA-modified electrodes. The plot shows the titration of TBP onto a 20% OCT-DNA monolayer (dark blue), a 50% OCT-DNA monolayer (blue) a 90% OCT-DNA monolayer (light blue), a low-density thiol monolayer (green), and a high-density thiol monolayer (red), as determined electrochemically. The signal remaining was determined through the quantification of the area of the anodic peak of a CV obtained at a scan rate of 100 mV/s. CVs were obtained with 2 μM daunomycin in Tris buffer (10 mM Tris, 100 mM KCl, 2.5 mM $MgCl_2$, 1 mM $CaCl_2$, pH 7.6). TBP is detectable with the OCT-DNA monolayer at concentrations as low as 4 nM (at which there is a greater than 15% signal decrease), which is near the K_D of the protein (3.3 nM); both high-density and low-density thiol monolayers have a negligible signal decrease at this protein concentration. Error bars represent the standard deviation obtained over nine replicates of each type of DNA-modified electrode.

The electrochemically derived TBP/OCT-DNA binding isotherm could not be fit well to a simple Langmuir thermodynamics model, indicating some form of cooperative TBP binding. We therefore analyzed the data according to the Frumkin-Fowler-Guggenheim (FFG) model,[33, 34, 43, 44] which accounts for lateral interactions on a surface. Using Eq. (2), a plot of log[θ/(1-θ)C] *vs.* θ gives a straight line (Figure 2.12).

$$\frac{\theta}{1-\theta}e^{2\theta a} = \beta C \qquad (2)$$

In this equation, θ is the fractional surface coverage (i.e., $\Gamma_{\text{TBP bound}}/\ \Gamma_{\text{TBP binding sites}}$), C is the solution concentration (M) of TBP, β is the adsorption equilibrium constant, and a is the lateral interaction or Frumkin coefficient. From this fit, values for the lateral interaction coefficient, a, and the adsorption equilibrium constant, β, were found to be 0.2 and 30 μM, respectively. The positive a value obtained indicates repulsive sorbent/sorbate lateral interactions. A repulsive lateral interaction on the surface is consistent with the steric presence that bound TBP exerts on DNA duplexes, impeding the binding of additional TBP proteins, as kinked TBP-bound helices likely impede binding of TBP to adjacent sequences. From the determined value of β (the adsorption equilibrium constant), $ln(\beta)$ can be used to characterize the free adsorption energy of the protein, ΔG_A, which provides the difference in free energy of TBP between its solution state and adsorbed state. The value for ΔG_A can be determined from Eq. (3):

$$\Delta G_A = -RTln(\beta) \qquad (3)$$

where R is the molar gas constant.[45-47] The free adsorption energy of the TBP protein on the low-density DNA monolayer is determined to be 42 kJ/mol. This positive free adsorption energy is not uncommon for charged molecules adsorbing onto a charged surface.[34]

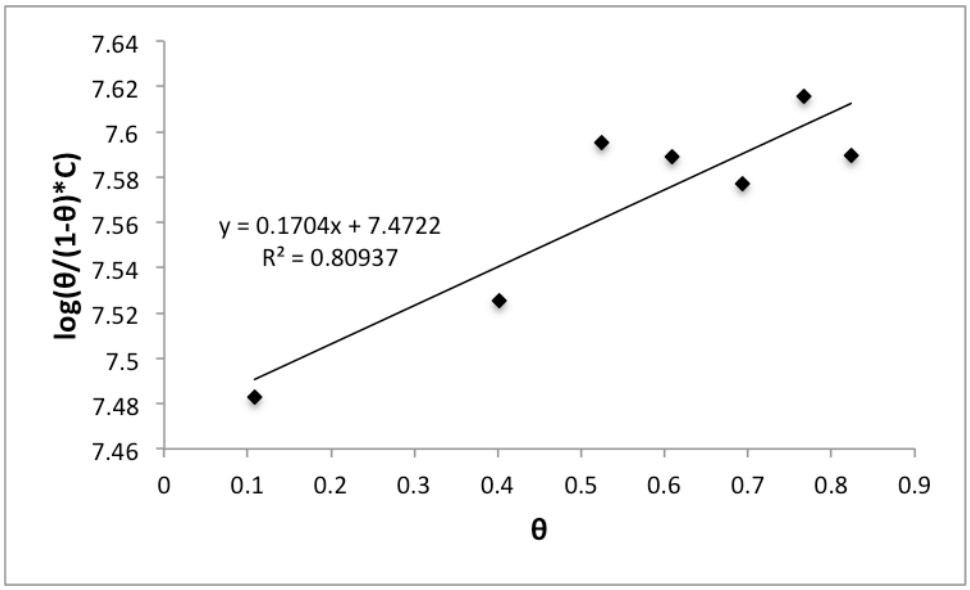

Figure 2.12 Linear fit of TBP titration data to the Frumkin-Fowler-Guggenheim adsorption isotherm. To determine the Frumkin coefficient (*a*) and the adsorption equilibrium constant (β) from the previous titration data, a plot of log[θ/(1-θ)C] versus the fractional surface coverage (θ), where C is the solution concentration of TBP is constructed. The linear fit of the data is shown, from which the two desired parameters are extrapolated.

Given the anti-cooperative nature of TBP binding observed upon thermodynamic investigations of this protein binding to OCT-DNA monolayers, we also investigated the relative kinetics of TBP binding to these monolayers and to thiolated DNA films. Rotating disk electrode (RDE) experiments were undertaken to determine the binding kinetics of TBP on both high density thiol-DNA and low-density OCT-DNA monolayers. RDEs remove diffusion as a factor when determining kinetics of a system.[44, 48] The loss of an electrochemical DM signal upon TBP binding over time therefore reports on the kinetics of protein binding. Because the number of TBP binding sites is fixed, the solution concentration of protein is in large enough excess to be unaffected by the amount of protein bound to the surface, and the rate of TBP diffusion to the surface is removed as a factor, we can analyze the kinetics of TBP binding to the surfaces with a Langmuir kinetics model. As is evident in Figure 2.13, which shows the decrease in charge determined from the area of the reductive peak plotted as a function of time, the rate of signal decrease for both the high density and ultra low-density monolayers upon TBP binding is almost identical. As is apparent in the figure, the RDEs produce similar overall signal attenuations to stationary electrodes for both types of DMEs. When the data are fit to this Langmuir equation for protein binding kinetics, the k_{obs} for high density monolayers was determined to be 6.1×10^{-3} s^{-1}; likewise, for the ultra low density monolayers, the k_{obs} was determined to be 6.1×10^{-3} s^{-1}. This indicates that protein binding to DMEs is a fairly slow process. Additionally, the rate of protein binding is unaffected by accessibility; only the amount of signal attenuation is dependent on DNA helix accessibility.

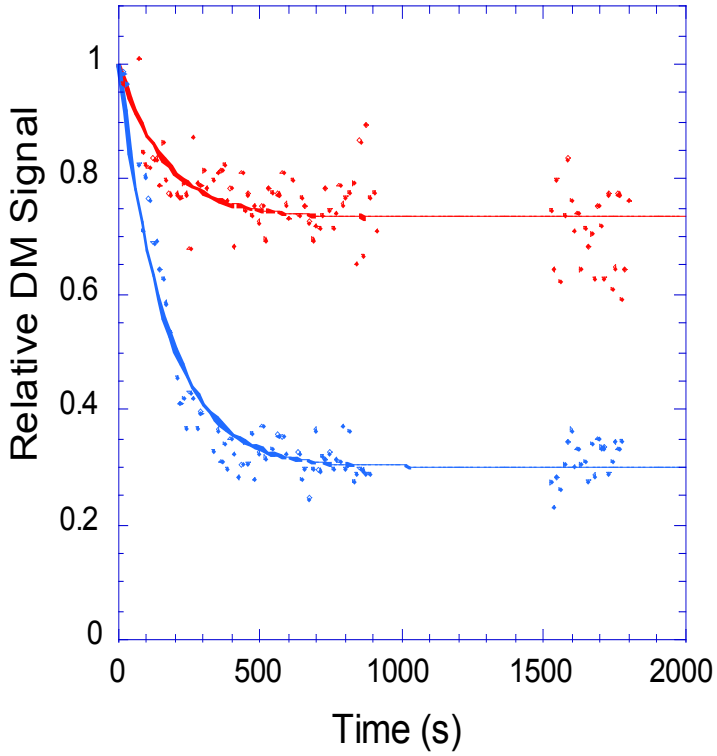

Figure 2.13 Kinetics of TBP binding to DNA-modified electrodes. The kinetics of TBP binding to both OCT-DNA monolayers and high density monolayers are determined electrochemically at a gold rotating disk electrode surface. Electrodes are rotated at 400 rpm, with 2 μM daunomycin in Tris buffer (10 mM Tris, 100 mM KCl, 2.5 mM $MgCl_2$, 1 mM $CaCl_2$, pH 7.6). TBP (75 nM) is added, and sequential CV scans are obtained at 100 mV/s. The relative DM signal is obtained through the quantification of the anodic CV peak and subsequent normalization to the value obtained for time=0. Curves for high-density thiol DNA (red) and low density OCT-DNA (blue) monolayers are shown. The data are fit to a Langmuir kinetics model based on exponential decay, which shows that the rates of TBP binding to both types of monolayers are essentially the same.

When thermodynamic and kinetic data are evaluated together, a model for TBP binding to DMEs becomes apparent. Based on the repulsive lateral interactions on the surface, the positive value for the free energy of adsorption and the relatively slow rate of TBP binding to both OCT-DNA and thiol-DNA films, TBP likely binds primarily to surface-exposed sequences. This conclusion is further supported by the significantly lower detection limits for the low-density OCT-DNA films as compared to the high-density thiol-DNA films. The low-density OCT-DNA monolayers have significantly more solution-exposed TBP binding sites than the thiol-DNA monolayers. This model for TBP binding is also consistent with the kinetics that are independent of surface coverage; only exposed sequences are available, and there are relatively fewer of them in tightly-packed films. This model of protein binding supports the utility of OCT-DNA monolayers for biomolecule detection, as the large amount of buffer-exposed helices aids TBP binding to the monolayers.

Conclusions

A novel method of DNA assembly to form DNA-modified surfaces for the electrochemical detection of biomolecules has been developed. The copper-free click-based strategy described here allows for the formation of low-density, more evenly spaced monolayers, while maintaining surface passivation against the redox reporter. Both electrochemical and imaging methods have been used to characterize these monolayers. This platform facilitates DNA-mediated CT and is thus extremely sensitive to perturbations in the DNA, providing exquisite electrochemical discrimination between well matched and mismatched DNA duplexes. Additionally, this platform provides greater sensitivity to protein binding events than conventional high-density films due to the larger number of accessible, solution-exposed binding sites. In particular, here, low-density films allow for the detection of as little as 4 nM TBP. The enhanced detection with OCT-DNA films adds another sensitive detection tool to the toolbox of electrochemical DNA CT-based detection strategies.

References

1. Cederquist, K. B., and Kelley, S. O. (2012) Nanostructured biomolecular detectors: pushing performance at the nanoscale, *Curr. Opin. Chem. Biol. 16*, 415-421.

2. Drummond, T. G., Hill, M. G., and Barton, J. K. (2003) Electrochemical DNA sensors, *Nat. Biotechnol. 21*, 1192-1199.

3. Gooding, J. J. (2002) Electrochemical DNA Hybridization Biosensors, *Electroanalysis 14*, 1149-1156.

4. Lord, H., and Kelley, S. O. (2009) Nanomaterials for ultrasensitive electrochemical nucleic acids biosensing, *J. Mat. Chem. 19*, 3127-3134.

5. Mikkelsen, S. R. (1996) Electrochecmical biosensors for DNA sequence detection, *Electroanalysis 8*, 15-19.

6. Slinker, J. D., Muren, N. B., Gorodetsky, A. A., and Barton, J. K. (2010) Multiplexed DNA-modified electrodes, *J. Am. Chem. Soc. 132*, 2769-2774.

7. Wang, J. (2006) Electrochemical biosensors: towards point-of-care cancer diagnostics, *Biosens. Bioelectron. 21*, 1887-1892.

8. Kelley, S. O., Boon, E. M., Barton, J. K., Jackson, N. M., and Hill, M. G. (1999) Single-base mismatch detection based on charge transduction through DNA, *Nucleic Acids Res. 27*, 4830-4837.

9. Boon, E. M., Ceres, D. M., Drummond, T. G., Hill, M. G., and Barton, J. K. (2000) Mutation detection by electrocatalysis at DNA-modified electrodes, *Nat. Biotechnol. 18*, 1096-1100.

10. Boon, E. M., Livingston, A. L., Chmiel, N. H., David, S. S., and Barton, J. K. (2003) DNA-mediated charge transport for DNA repair, *Proc. Natl. Acad. Sci. USA 100*, 12543-12547.

11. Boon, E. M., Salas, J. E., and Barton, J. K. (2002) An electrical probe of protein-DNA interactions on DNA-modified surfaces, *Nat. Biotechnol. 20*, 282-286.

12. Gorodetsky, A. A., Buzzeo, M. C., and Barton, J. K. (2008) DNA-mediated electrochemistry, *Bioconjug. Chem. 19*, 2285-2296.

13. Gorodetsky, A. A., Ebrahim, A., and Barton, J. K. (2008) Electrical detection of TATA binding protein at DNA-modified microelectrodes, *J. Am. Chem. Soc. 130*, 2924-2925.

14. Guo, X., Gorodetsky, A. A., Hone, J., Barton, J. K., and Nuckolls, C. (2008) Conductivity of a single DNA duplex bridging a carbon nanotube gap, *Nat. Nanotechnol. 3*, 163-167.

15. Chen, C., Wang, W., Ge, J., and Zhao, X. S. (2009) Kinetics and thermodynamics of DNA hybridization on gold nanoparticles, *Nucleic Acids Res. 37*, 3756-3765.

16. Peterson, A. W., Heaton, R. J., and Georgiadis, R. M. (2001) The effect of surface probe density on DNA hybridization, *Nucleic Acids Res. 29*, 5163-5168.

17. Chrisey, L. A., Lee, G. U., and O'Ferrall, C. E. (1996) Covalent attachment of synthetic DNA to self-assembled monolayer films, *Nucleic Acids Res. 24*, 3031-3039.

18. Kelley, S. O., Barton, J. K., Jackson, N. M., and Hill, M. G. (1997) Electrochemistry of methylene blue bound to a DNA-modified electrode, *Bioconjug. Chem. 8*, 31-37.

19. Levicky, R., Herne, T. M., Tarlov, M. J., and Satija, S. K. (1998) Using Self-Assembly To Control the Structure of DNA Monolayers on Gold: A Neutron Reflectivity Study, *J. Am. Chem. Soc. 120*, 9787-9792.

20. Yu, H. Z., Luo, C. Y., Sankar, C. G., and Sen, D. (2003) Voltammetric procedure for examining DNA-modified surfaces: quantitation, cationic binding activity, and electron-transfer kinetics, *Anal. Chem. 75*, 3902-3907.

21. Mui, S., Boon, E. M., Barton, J. K., Hill, M. G., and Spain, E. M. (2001) Morphology of 15-mer Duplexes Tethered to Au(111) Probed Using Scanning Probe Microscopy, *Langmuir. 17*, 5727-5730.

22. Murphy, J. N., Cheng, A. K., Yu, H. Z., and Bizzotto, D. (2009) On the nature of DNA self-assembled monolayers on Au: measuring surface heterogeneity with

electrochemical in situ fluorescence microscopy, *J. Am. Chem. Soc. 131*, 4042-4050.

23. Folkers, J. P., Laibinis, P. E., and Whitesides, G. M. (1992) Self-assembled monolayers of alkanethiols on gold: comparisons of monolayers containing mixtures of short- and long-chain constituents with methyl and hydroxymethyl terminal groups, *Langmuir 8*, 1330-1341.

24. Hobara, D., Sasaki, T., Imabayashi, S.-i., and Kakiuchi, T. (1999) Surface Structure of Binary Self-Assembled Monolayers Formed by Electrochemical Selective Replacement of Adsorbed Thiols, *Langmuir 15*, 5073-5078.

25. Love, J. C., Estroff, L. A., Kriebel, J. K., Nuzzo, R. G., and Whitesides, G. M. (2005) Self-assembled monolayers of thiolates on metals as a form of nanotechnology, *Chem. Rev. 105*, 1103-1169.

26. Sellers, H., Ulman, A., Shnidman, Y., and Eilers, J. E. (1993) Structure and binding of alkanethiolates on gold and silver surfaces: implications for self-assembled monolayers, *J. Am. Chem. Soc. 115*, 9389-9401.

27. Stranick, S. J., Parikh, A. N., Tao, Y. T., Allara, D. L., and Weiss, P. S. (1994) Phase Separation of Mixed-Composition Self-Assembled Monolayers into Nanometer Scale Molecular Domains, *J. Phys. Chem. 98*, 7636-7646.

28. Tamada, K., Hara, M., Sasabe, H., and Knoll, W. (1997) Surface Phase Behavior of n-Alkanethiol Self-Assembled Monolayers Adsorbed on Au(111): An Atomic Force Microscope Study, *Langmuir 13*, 1558-1566.

29. Ulman, A. (1996) Formation and Structure of Self-Assembled Monolayers, *Chem. Rev. 96*, 1533-1554.

30. Devaraj, N. K., Miller, G. P., Ebina, W., Kakaradov, B., Collman, J. P., Kool, E. T., and Chidsey, C. E. (2005) Chemoselective covalent coupling of oligonucleotide probes to self-assembled monolayers, *J. Am. Chem. Soc. 127*, 8600-8601.

31. Agard, N. J., Prescher, J. A., and Bertozzi, C. R. (2004) A strain-promoted [3 + 2] azide-alkyne cycloaddition for covalent modification of biomolecules in living systems, *J. Am. Chem. Soc. 126*, 15046-15047.

32. Baskin, J. M., and Bertozzi, C. R. (2007) Bioorthogonal Click Chemistry: Covalent Labeling in Living Systems, *QSAR & Comb. Sci. 26*, 1211-1219.

33. Trasatti, S. (1974) Acquisition and analysis of fundamental parameters in the adsorption of organic substances at electrodes, *J. Electroanal. Chem. and Interfacial Electrochem. 53*, 335-363.

34. Goyne, K. W., Chorover, J., Zimmerman, A. R., Komarneni, S., and Brantley, S. L. (2004) Influence of mesoporosity on the sorption of 2,4-dichlorophenoxyacetic acid onto alumina and silica, *J. Colloid Interface Sci 272*, 10-20.

35. Huisgen, R. (1961) Proceedings of the Chemical Society. October 1961, *Proc. Chem. Soc.* 357-396.

36. Ceres, D. M., Udit, A. K., Hill, H. D., Hill, M. G., and Barton, J. K. (2007) Differential ionic permeation of DNA-modified electrodes, *J. Phys. Chem. B 111*, 663-668.

37. Steel, A. B., Herne, T. M., and Tarlov, M. J. (1998) Electrochemical quantitation of DNA immobilized on gold, *Anal. Chem. 70*, 4670-4677.

38. Anson, F. C., and Rodgers, R. S. (1973) Electrode kinetics for a simple redox reaction with adsorbed reactant: The reduction of $Cr(OH_2)_3(NCS)_3$ at mercury electrodes, *J. Electroanal. Chem. and Interfacial Electrochem. 47*, 287-309.

39. Jackson, N. M., and Hill, M. G. (2001) Electrochemistry at DNA-modified surfaces: new probes for charge transport through the double helix, *Curr. Opin. Chem. Biol. 5*, 209-215.

40. Palanti, S., Marrazza, G., and Mascini, M. (1996) Electrochemical DNA Probes, *Anal. Lett. 29*, 2309-2331.

41. Nikolov, D. B., Hu, S. H., Lin, J., Gasch, A., Hoffmann, A., Horikoshi, M., Chua, N. H., Roeder, R. G., and Burley, S. K. (1992) Crystal structure of TFIID TATA-box binding protein, *Nature 360*, 40-46.

42. Gorodetsky, A. A., Hammond, W. J., Hill, M. G., Slowinski, K., and Barton, J. K. (2008) Scanning electrochemical microscopy of DNA monolayers modified with Nile Blue, *Langmuir 24*, 14282-14288.

43. Fowler, R., and Guggenheim, E. A. (1965) *Statistical Thermodynamics*, Cambridge Univ. Press: London.

44. Vendra, V. K., Wu, L., and Krishnan, S. (2010) Nanostructured Thin films and Surfaces, In *Nanomaterials for the Life Sciences* (Kumar, C. S. S. R., Ed.), pp 1-54, Wiley-VCH, Weinheim.

45. Bard, A. J., Inzelt, G., and Scholz, F. (2012) *Electrochemical Dictionary*, 2nd ed.

46. Butt, H. J., Graf, K., and Kappl, M. (2006) *Physics and Chemistry of Interfaces*, 2nd ed., Wiley-VCH, Federal Republic of Germany.

47. Herne, T. M., and Tarlov, M. J. (1997) Characterization of DNA Probes Immobilized on Gold Surfaces, *J. Am. Chem. Soc. 119*, 8916-8920.

48. Anson, F. C. (1968) Electrochemistry, *Annu. Rev. Phys. Chem. 19*, 83-110.